Spin-polarized cation monovacancies in wurtzite structure semiconductors: first-principles study

著者	Widianto Muhammad Yusuf Hakim, Kadarisman Hana Pratiwi, Yatmeidhy Amran Mahfudh, Saito Mineo
著者別表示	斎藤 峯雄
journal or publication title	Japanese Journal of Applied Physics
volume	59
number	7
page range	071001
year	2020-06-10
URL	http://doi.org/10.24517/00065298

doi: 10.35848/1347-4065/ab9654

Creative Commons : 表示 - 非営利 - 改変禁止
http://creativecommons.org/licenses/by-nc-nd/3.0/deed.ja

Spin-Polarized Cation Monovacancies in Wurtzite Structure Semiconductors: First-principles study

Muhammad Yusuf Hakim Widianto[1 *], Hana Pratiwi Kadarisman[1], Amran Mahfudh Yatmeidhy[1] and Mineo Saito[2]

[1] *Graduate School of Natural Science and Technology, Kanazawa University, Kanazawa 920-1192, Japan*
[2] *Faculty of Mathematics and Physics, Institute of Science and Technology, Kanazawa University, Kanazawa 920-1192, Japan*

We study spin-polarized cation vacancies in wurtzite structure semiconductors (BeO, ZnO, ZnS, CdS, BN, AlN, GaN and GaP) by using first-principles calculations based on the density functional theory. We find that C_{3v} geometries are the most stable and are spin-polarized. Two majority spin electrons occupying the defect E level lead to the magnetic moment of 2 μ_B in the case of II-VI semiconductors. On the contrary, in the case of III-V semiconductors, three majority spin electrons occupying the defect E and A_1 levels induce the magnetic moment of 3 μ_B. The spin polarization of cation vacancies in oxides and nitrides are found to be stable compared with other cation vacancies in II-VI and III-V semiconductors, respectively. We clarify that the effect of the symmetry lowering from C_{3v} to C_s is small and thus confirm that the spin polarized C_{3v} geometries are the most stable.

1. Introduction

Diluted magnetic semiconductors have attracted scientifical interests because of spintronics applications.[1–3] The magnetism is induced by various reasons, i.e., the secondary phase, intentional doping, and lattice defects.[4] Recently, the spin polarization in intrinsic defects in wide-gap semiconductors was found to raise high-temperature ferromagnetism. In particular, it is observed in the cases of oxides (HfO_2,[5] TiO_2,[6] SnO_2,[7] ZnO,[8,9] MgO[10]) and nitrides (AlN,[11] BN,[12] and GaN[13]). Low-temperature ferromagnetism was found for ZnS,[14] CdS[13,15] and GaP.[16] In those systems, it is suggested that cation vacancies cause magnetic moments. Formation of cation vacancies is detected by using electron microscopy, X-ray absorption spectroscopy and positron annihilation spectroscopy.[17–20] The robust spin polarization of vacancies is clarified by theoretical studies based on the density functional theory.[21–26] These vacancies form *sp*-hybridized electronic states and therefore the magnetism is induced

*E-mail: mwidianto@cphys.s.kanazawa-u.ac.jp

in d^0 systems without localized (d and f) atomic orbitals. Hence, it is important to study the mechanism of vacancy-induces spin-polarization.

In this paper, we systematically study the spin polarization of cation vacancies in the wurtzite structure semiconductors (BeO, ZnO, ZnS, CdS, BN, AlN, GaN, and GaP). We find that the spin density is localized at four near anions and first-row anions (oxygen and nitrogen anions) induce large spin polarization energies. The magnetic moment of 2 μ_B is found in II-VI semiconductors. This is due to the fact that the defect E level is occupied and unoccupied by majority spin and minority spin electrons, respectively. On the other hand, the magnetic moment of 3 μ_B is induced in III-V semiconductors due to the fact that the E and A_1 levels are occupied and unoccupied by majority spin and minority spin electrons, respectively. We check the possibility of the occurrence of symmetry lowering from C_{3v} which reduces the spin multiplicity. We find that the energy gain induced by the symmetry lowering is small, therefore we conclude that the above mentioned spin-polarized C_{3v} state is the most stable.

2. Method of Calculations

We carry out first-principles calculations based on the generalized gradient approximation[27] within the density functional theory. We use the PHASE/0 code,[28] where ultrasoft pseudopotentials and plane waves are used. Optimized lattice constants for pristine wurtzite structures of BeO, ZnO, ZnS, CdS, BN, AlN, GaN, and GaP are shown in Table I. We introduce a single cation vacancy in the 128-site wurtzite supercell (Fig. 1). The cutoff energies of the wavefunctions and charge density are 25 Rydberg and 225 Rydberg, respectively. We optimize the geometries under the condition that the atomic forces are less than 0.005 eV/Å. The $3 \times 3 \times 3$ mesh of k-points is used for supercell calculations. When we increase the k-points up to $7 \times 7 \times 7$ mesh, the optimized bond length varies within 0.001 Å and the bond angle varies within 0.01°.

We analyze the wavefunctions at the Γ point in the Brillouin zone of the supercell and clarify the irreducible representations of the defect levels. We use a projection operator method to identify the irreducible representations of the defect levels, which was described in previous papers.[29,30]

3. Results and Discussion

3.1 II-VI Semiconductors

We first study cation vacancies in oxide semiconductors (ZnO and BeO). The most stable geometries are found to have the C_{3v} symmetry and are spin polarized. As the density of states

(DOS) in Fig. 2(a) of BeO shows, the A_1 defect level of the minority spin is located just below the Fermi level and is thus occupied. The defect E level of the minority spin is located above the Fermi level and is unoccupied (The irreducible representations of the above mentioned levels are identified by analyzing the wavefunctions at the Γ point in the supercell). Since the E level is occupied by only majority spin electrons, the calculated magnetic moment is 2 μ_B. It is noted that the DOS of the defect level is somewhat broad, which is caused by the fact that we use the finite size of the supercell, so the band dispersion of the defect level arises artificially. When we use a larger supercell, we find that the dispersion becomes small.

In the case of ZnO, the calculated magnetic moment is 1.71 μ_B. This non-integer value originates from the finite dispersions of the defect A_1 and E levels as the DOS in Fig 2(b) shows. When we use a sufficiently large unit cell, it is expected that the DOS of the defect level becomes narrower and the magnetic moment becomes the integer (2 μ_B). Non-integer values of the magnetic moments were also obtained in past theoretical calculations.[32,33]

The oxygen-oxygen atomic distances, r_a (r_b) in Fig. 1, is 10.3% (10.1%) larger than the ideal value (the value in the pristine crystal) in the case of ZnO. The increases of the atomic distances are due to the outward relaxations of the four oxygen atoms. In the case of BeO, r_a and r_b are 11.2% and 10.1% larger than the ideal distance, respectively (Table II). As a result, the bond angles of the near four oxygen atoms become larger than the sp^3 hybridization angle (109.5°) as Table II shows; The bond angles θ ($\overline{\theta}$) are 115.2° (116.6°) and 116.0° (116.7°) for BeO and ZnO, respectively, where θ is the bond angle of the fourth anion and $\overline{\theta}$ is the average value of the three bond angles of the first anion (The locations of the first and fourth anions are indicated in Fig. 1).

The spin densities in ZnO and BeO are found to be localized at the near four oxygen atoms (Fig. 3(a) and 3(b)). The spin density mainly consists of the oxygen *p*-orbitals and the *s*-component is small as Fig. 3(a) and 3(b) shows. The small *s*-component originates from the fact that the defect E level occupied by only majority spin electrons contains small *s*-component. This small *s*-component can be confirmed by analyzing the partial density of states (PDOS); we find that the defect E levels of the minority spin have small *s*-component (Fig. 2(a) and 2(b)). This small *s*-component is due to the fact that the bond angles of the near oxygen atoms is substantially larger than the sp^3 bond angle.

In the case of cation vacancies in sulfide semiconductors (ZnS and CdS), the stable structures have C_{3v} symmetries and are spin polarized as in the case of oxides. The calculated magnetic moments are 1.66 μ_B and 1.95 μ_B for ZnS and CdS, respectively. These non-integer values are due to the finite dispersion of the defect A_1 and E levels as in the case of ZnO.

These results of non-integer values are consistent with those in the past calculations.[34–36)]

In sharp contrast with the oxides, the bond angles of the near four sulfur atoms in sulfides are close to the sp^3 bond angle (Table II). The bond angles θ ($\bar{\theta}$) are 109.5° (110.5°) and 112.4° (113.1°) for ZnS and CdS, respectively. These bond angles are due to the fact that the outward relaxations of the sulfur atoms are small. The sulfur-sulfur atomic distance, r_a (r_b), in ZnS is 1.1% (1.0%) larger than the ideal distance. In the case of CdS, the atomic distance, r_a (r_b), is 5.3% (2.3%) larger than the value of the ideal value (Table II).

Since the bond angles are close to the sp^3 one, the spin density localized at four near anions contain more *s*-components than that in the case of the oxides, as shown in Fig. 3(c) and 3(d). This is due to the defect E level occupied by majority spin electrons contain large *s*-component. Indeed, the PDOS of sulfides for the minority spin (Fig. 2(c) and 2(d)) shows that the defect E levels have a large *s*-component than those in the case of oxides. The large *s*-component originates from the fact that the bond angles of the near sulfur atoms are close to the sp^3 bond angle.

We next evaluate the spin polarization energy (ΔE_p) which is the energy of the non-magnetic state measured from the energy of the spin-polarized state (Table II). The energies are found to be large in the case of oxides; The energies are 0.35 eV and 0.04 eV for BeO and ZnO, respectively. On the other hand, the spin polarization energies of the sulfides are found to be small; The energies are very small for ZnS and CdS, respectively (Table II). Since we have found that the spin density is localized at the near four cation atoms, we expect that the large spin polarization energies in the oxides are due to the fact that the atomic radii of oxygen is much smaller than that of sulfur as previous studies indicated.[34,35)] Therefore, we conclude that oxides are good candidates for vacancy-induces spin-polarization materials.

3.2 III-V Semiconductors

Next we study cation vacancies in nitride semiconductors (BN, AlN, and GaN). In the optimized geometries, the symmetries are C_{3v}. The magnetic moments are found to be 3 μ_B: The defect E and A_1 levels are occupied by three majority spin electrons and are unoccupied by minority spin electrons as the DOS in Fig. 2(e), 2(f) and 2(g) show (The E level splits into two peaks in the DOS. This is due to the artificial band dispersion of the supercell model; i.e., the E level is doubly degenerated at the Γ point but splits into two at general *k*-points.). These results are in sharp contrast with the results for II-VI semiconductors; The A_1 level is occupied by minority and majority spin electrons and the magnetic moment is 2 μ_B.

The outward relaxations are found to occur at the near four nitrogen atoms. As a result,

r_a and r_b of BN (AlN) is 9.4% and 9.2% (11.6% and 11.1%) larger than the ideal distance. In the case of GaN, r_a and r_b are 9.2% and 9.4% larger than the ideal value, respectively (Table II). As a result, the bond angles of near four nitrogen atoms are close to the sp^2 hybridization bond angle as is seen in Table II: The bond angles θ ($\bar{\theta}$) are 114.1° (114.1°), 116.1° (117.4°) and 115.0° (115.0°) for BN, AlN, and GaN, respectively.

The spin densities are found to be localized at the nitrogen atoms (Fig. 3(e), 3(f) and 3(g)) and mainly consist of the *p*-orbitals of the nitrogen atoms and the contributions of the *s*-orbitals are small. This is due to the fact that the defect E and A_1 levels occupied by majority spin contains *p*-orbitals and the *s*-component is small. Indeed, the PDOS in Fig. 2(e), 2(f) and 2(g) show that the defect E and A_1 levels have small *s*-components. These small *s*-components are due to the fact that the bond angles of the four near anions are substantially larger than the sp^3 bond angle.

We here compare phosphide and nitride; we clarify the energetical stability of cation vacancies in the two cases. GaP forms the zinc blende structure[16)] and the wurtzite structure is achieved in the case of nanowires.[37)] However, since our purpose is to study the chemical trend for the anions in III-V semiconductors, we study the wurtzite structure of the GaP bulk. The stable symmetry, spin-polarized state, and the magnetic moment in the case of GaP are the same as those in nitride semiconductors. The defect E and A_1 levels are occupied (unoccupied) by three majority (minority) spin electrons, as the Fig. 2(h) indicates. The bond angle θ ($\bar{\theta}$) is 107.6° (107.4°) for GaP and is thus close to the sp^3 bond angle (109.5°) due to the fact small relaxation of the near four phosphorus atoms (Table II). This is due to the fact that the outward relaxation is small and thus the atomic distance, r_a (r_b), is only 1.7% (5.5%) larger than the ideal value.

The spin density is localized at the four phosphide atoms near vacancies as is seen in Fig. 3(h). Since the bond angle is close to the sp^3 bond angle, the spin density contains a large *s*-component compared with the case of nitrides (Fig. 3(g) and 3(h)). This feature is due to the fact that the defect E and A_1 levels contain more *s*-components than those of nitrides, which is confirmed by the fact that the defect E and A_1 levels of the minority spin contain large *s*-components as the PDOS (Fig. 2(h)) shows. The large *s*-component is due to the fact that the bond angles of the near four phosphorus atoms are close to sp^3 bond angle.

Next we evaluate the spin polarization energies of cation vacancies in nitrides. The energies are 0.19 eV, 0.83 eV and 0.48 eV for BN, AlN, and GaN, respectively. On the other hand, the spin polarization energy of GaP is very small. Since the spin density is localized at the near four anions, the difference in the spin polarization energies between nitrides and phos-

phide is expected to be due to the fact that the nitrogen atom has a smaller atomic radii than the phosphorus atom as is discussed in a previous study.[24] Therefore, we conclude that the spin polarized state of the cation vacancy is stable in nitrides. In a previous section, we also concluded that the cation vacancy is stable in oxides. These conclusions are consistent with experimental results that high-temperature ferromagnetisms are found in cation vacancies of oxides and nitrides.[8,9,13,20,21]

3.3 Symmetry lowering Effect

So far, we have assumed that the symmetry of the vacancies is C_{3v} and clarified that the spin-polarized states are stable, in particular, for cation vacancies of oxides and nitrides. When the symmetry of C_{3v} is lowered, the E level splits, then the magnetic moments are expected to decrease. Thus, we here study the possibility of the occurrence of the symmetry lowering.

First, we study ZnO. As was discussed, in the C_{3v} geometry, two majority spin electrons occupy the E defect level and thus the spin state is triplet (S=1). The Jahn-Teller (JT) effect is expected to lower the symmetry from C_{3v} to C_s and the E level splits into A' and A" (Fig. 4). Due to the splitting of the E level, the system becomes the spin singlet (S=0) since the two electrons occupy the lower level (see Fig. 4). There are two types of the symmetry lowering distortions, i.e., pairing and depairing distortions as is illustrated in Fig. 5. In the case of the pairing distortion, $r_{a'}$ is smaller than $r_{b'}$ and vice versa in the case of the deparing distortion. We tabulate the atomic distances in the low symmetry geometry in Table III. We find that the pairing relaxation occurs in the case of ZnO.

Here, we consider the wavefunctions based on a simplified model which includes dangling bond orbitals, χ_i, of the four near anions (i=1-4) forming the tetrahedron; the fourth anion dangling bond orbital is located at the top of the tetrahedron and the other three (i=1-3) are located on the basal plane (Fig. 1). Two wavefunctions, $\psi_1 = \frac{1}{\sqrt{6}}(2\chi_2 - \chi_1 - \chi_3)$ and $\psi_2 = \frac{1}{\sqrt{2}}(\chi_1 - \chi_3)$, belong to the E representation in the C_{3v} symmetry. When the symmetry is lowered to C_s, ψ_1 and ψ_2 belong to A' and A", respectively (Since χ_4 belongs to A', it can be mixed with ψ_1 but the mixing is found to be very small as Fig. 4 shows). When the pairing distortion occurs, the A' level is lower than the A" level since the distance between the first and third atoms become small (Fig. 5). We confirm this energetical order by analyzing the wavefunctions obtained from the density functional calculation (Fig. 4). We find that the JT distortions are very small; the difference between $r_{a'}$ and $r_{b'}$ is only 0.007 Å (Table III). As a result, the JT energy which is the energy of the low spin (spin singlet) C_{3v} symmetry measured from the energy of the low spin (spin singlet) C_s symmetry is small (ΔE_1 = 0.01 eV),

as Table III shows. Therefore, the spin triplet state of the C_{3v} symmetry has 0.03 eV lower energy than the spin singlet C_s symmetry (As Table III shows, $\Delta E_2 = \Delta E_p - \Delta E_1 = 0.03$ eV).

We next study the GaN case. The defect A_1 and E levels are occupied (unoccupied) by majority (minority) spin electrons as was mentioned in the previous section and thus the spin state is quartet (S=3/2). The A_1 level has 0.01 eV lower energy than the E level (Fig. 4). In our four-anion dangling-bond model, the wavefunction of the A_1 level is $\psi_3 = \frac{1}{\sqrt{3+\alpha^2}}(\chi_1 + \chi_2 + \chi_3 - \alpha\chi_4)$, where α is a constant. Due to the symmetry lowering from C_{3v} to C_s, the E level splits into A' (ψ_1) and A" (ψ_2) as in the case of ZnO and A_1 (ψ_3) becomes A'. In this system, we conclude that the depairing distortion occurs based on the results of the density functional calculation. As a result, the A" level is lower than the A' level (Fig. 4). The A' level originating from the A_1 level in the C_{3v} symmetry has lower energy than the above two levels. Therefore, when we restrict our calculation within the spin doublet (S=1/2), the A' level is occupied by two electrons and the A" level is occupied by a single electron. We find that the the difference between $r_{a'}$ and $r_{b'}$ is small (0.006 Å) as in the case of ZnO but the difference between $r_{c'}$ and $r_{d'}$ is 0.008 Å, which is larger than that (0.002 Å) in the case of ZnO (The definitions of $r_{c'}$ and $r_{d'}$ are given in Fig. 5). We find that the symmetry lowering energy which is the energy of the low spin (spin doublet) C_{3v} symmetry measured from the energy of the low spin (spin doublet) C_s symmetry (ΔE_1) is 0.23 eV, which is larger than that in ZnO (0.01 eV). However, we find that the spin quartet C_{3v} state has 0.25 eV lower energy than the spin doublet C_s state. This stability of the spin quartet C_{3v} is due to the fact that the spin polarized energy (ΔE_p) is large (0.48 eV) in GaN as is seen in Table II. In both cases of ZnO and GaN, the energies (ΔE_1) induced by the symmetry lowering are found to be smaller than those of the spin polarized energies (ΔE_p) and thus the spin polarized C_{3v} state is the most stable.

Small symmetry lowering distortion of the depairing type is also found in AlN and BeO (Table III). As a result, the C_{3v} geometry of the spin quartet state has much lower energy than the doublet C_s geometry of the spin doublet state (Table III). Based on the results of the present DFT calculations, we find that the symmetry lowered structure of BN, GaP, ZnS and CdS are unstable.

We have clarified that the symmetry lowering effect is very small in cation vacancies in II-VI and III-V semiconductors. Therefore, we conclude that the spin singlet (doublet) C_s geometries are metastable or unstable and thus the triplet (quartet) C_{3v} symmetries are the most stable in the case of II-VI (III-V) semiconductors. These results are in sharp contrast with the case of silicon neutral monovacancy.[38–40] The four nearest Si atoms are relaxed inwardly and

thus, the interactions between Si atoms become large. As a result, the JT distortion leads to the bonding of the dangling bonds and thus, the spin singlet state becomes the most stable.

4. Conclusion

We have studied cation vacancies in II-VI (oxides and sulfides) and III-V (nitrides and phosphides) wurtzite structure semiconductors by using spin-polarized DFT calculations. We find that the most stable structures have C_{3v} symmetries and are spin-polarized. The magnetic moments are 2 μ_B and 3 μ_B for II-VI and III-V semiconductors, respectively. The defect E level is occupied by two majority spin electrons and unoccupied by minority spin electrons in the II-IV semiconductors. In the case of III-V semiconductors, the defect E and A_1 levels are occupied (unoccupied) by three majority (minority) spin electrons. The spin polarization energies are large in the semiconductors consisting of first-row anions, i.e., oxides and nitrides. Finally, we study the possibility of the symmetry lowering distortion and find that the energy induced by the symmetrt lowering (ΔE_1) is smaller than the spin polarized energy (ΔE_p). Therefore, the spin polarized C_{3v} symmetry is the most stable.

5. Acknowledgment

This work was partly supported by Grants-in-Aid for Scientific Research (No. 17K05118) from the Japan Society for the Promotion of Science (JSPS). The computations in this research were performed using the supercomputers at the Institute for Solid State Physics (ISSP) at the University of Tokyo. The authors (M.Y.H.W, H.P.K and A.M.Y) acknowledges financial support from the Japanese Government (MEXT) Scholarship Program.

References

1) T. Dietl, H. Ohno, F. Matsukura, J. Cibert, and D. Ferrand, Science **287**, 1019 (2000).
2) H. Ohno, J. Appl. Phys. **113**, 136509 (2013).
3) Y. Ogawa, H. Akinaga, F. Takano, T. Arima, and Y. Tokura, J. Phys. Soc. Jpn. **73**, 2389-2392 (2004).
4) J. M. D. Coey, Solid State Mater. Sci. **10**, 83-92 (2006).
5) K. P. McKenna, and D. M. Ramo, Phys. Rev. B **92**, 205124 (2015).
6) N. H. Hong, J. Sakai, N. Poirot, and V. Brizé, Phys. Rev. B **73**, 132404 (2006).
7) N. H. Hong, N. Poirot, and J. Sakai, Phys. Rev. B **77**, 033205 (2008).
8) K. Potzger, S. Zhou, J. Grenzer, M. Helm, and J. Fassbender, Appl. Phys. Lett. **92**, 182504 (2008).
9) S. M. Evans, N. C. Giles, L. E. Halliburton, and L. A. Kappers, J. Appl. Phys. **103**, 043710 (2008).
10) A. Droghetti, C. D. Pemmaraju, and S. Sanvito, Phys. Rev. B **81**, 092403 (2010).
11) Y. Liu, L. Jiang, G. Wang, S. Zuo, W. Wang, and X. Chen, Appl. Phys. Lett. **100**, 122401 (2012).
12) P. Dev, Y. Xue, and P. Zhang, Phys. Rev. Lett. **100**, 117204 (2008).
13) C. Madhu, A. Sundaresan, and C. N. R. Rao, Phys. Rev. B **77**, 201306(R) (2008).
14) G. Zhu, S. Zhang, Z. Xu, J. Ma, and X. Shen, J. Am. Chem. Soc. **133**, 15605-15612 (2011).
15) D. Guo, H. Hua, Q. Yang, X. Li, and C. Hu, J. Phys. Chem. C **118**, 11426-11431 (2014).
16) T. A. Kennedy, N. D. Wilsey, J. J. Krebs and G. H. Stauss, Phys. Rev. Lett. **50**, 1281 (1983).
17) P. Zhan, W. Wang, C. Liu, Y. Hu, Z. Li, Z. Zhang, P. Zhang, B. Wang, and X. Cao, J. Appl. Phys. **111**, 033501 (2012).
18) W. Yan, Z. Sun, Q. Liu, Z. Li, Z. Pan, J. Wang, and S. Wei, Appl. Phys. Lett. **91**, 062113 (2007).
19) M. Maekawa, H. Abe, A. Miyashita, S. Sakai, S. Yamamoto, and A. Kawasuso, Appl. Phys. Lett. **110**, 172402 (2017).
20) M. Maekawa, S. Sakai, A. Miyashita, and A. Kawasuso, e-J. Surf. Sci. Nanotech. **16**, 347-350 (2018).
21) P. Dev and P. Zhang, Phys. Rev. B **81**, 085207 (2010).
22) M. Venkatesan, C. Fitzgerald, and J. M. D. Coey, Nature **430**, 630 (2004).

23) J. M. D. Coey, M. Venkatesan, P. Stamenov, C. B. Fitzgerald, and L. S. Dorneles, Phys. Rev. B **72**, 024450 (2005).

24) O. Volnianska and P. Boguslawski, Phys. Rev. B **83**, 205205 (2011).

25) O. Volnianska and P. Boguslawski, J. Phys. Condens. Matter. **22**, 073202 (2010).

26) I. S. Elfimov, S. Yunoki, and G. A. Sawatzky, Phys. Rev. Lett. **89**, 216403, (2002).

27) J. P. Perdew, K. Burke, and M. Ernzerhof, Phys. Rev. Lett. **77**, 3865 (1996).

28) T. Ohno, T. Yamamoto, T. Kokubo, A. Azami, Y. Sakaguchi, T. Uda, T. Yamasaki, D. Fukata, and J. Koga, SC '07: Proc. 2007 ACM/IEEE Conf. on Supercomputing, 2007 Article 57.

29) S. Minami, I. Sugita, R. Tomita, H. Oshima, and M. Saito, Jpn. J. Appl. Phys. **56**, 105102 (2017).

30) N. A. P. Namari and M. Saito, Jpn. J. Appl. Phys. **58**, 061003 (2019).

31) H. Ren, J. Jian, C. Chen, D. Pan, A. Ablat, Y. Sun, J. Li, R. Wu, Appl. Phys. A **116**, 185-191 (2014).

32) H. Peng, H. J. Xiang, S. Wei, S. Li, J. Xia, and J. Li, Phys. Rev. Lett. **102**, 017201 (2009).

33) M. Sargolzaei, N. Lotfizadeh, and R. Hayn, J. Appl. Phys. **109**, 073705 (2011).

34) W. Xiao, L. Wang, Q. Rong, G. Xiao, and B. Meng, J. Appl. Phys. **115**, 213905 (2014).

35) T. Chanier, I. Opahle, M. Sargolzaei, R. Hayn, and M. Lannoo, Phys. Rev. Lett. **100**, 026405 (2008).

36) J. P. Tang, L. L. Wang, H. J. Luo, W. Z. Xiao, Phys. Lett. A **377**, 572-576 (2013).

37) S. Assali, I. Zardo, S. Plissard, D. Kriegner, M. A. Verheijen, G. Bauer, A. Meijerink, A. Belabbes, F. Bechstedt, J. E. M. Haverkort, and E. P. A. M. Bakkers, Nano Lett. **13**, 1559 (2013).

38) G. A. Baraff, E. O. Kane, and M. Schlüter, Phys. Rev. B **21**, 5662 (1980).

39) O. Sugino and A. Oshiyama, Phys. Rev. Lett. **68**, 1858 (1992).

40) M. Saito, A. Oshiyama, and S. Tanigawa, Phys. Rev. B **44**, 10601 (1991).

Table I. Lattice constants of wurtzite structures.

Systems	a (Å)	c (Å)
BeO	2.718	4.389
ZnO	3.305	5.285
ZnS	3.909	6.349
CdS	4.332	6.745
BN	2.559	4.239
AlN	3.145	5.029
GaN	3.144	5.119
GaP	3.842	6.335

Table II. Optimized geometries. The bond angles, θ, and atomic distances, r_a and r_b are defined in Figure 1. $\overline{\theta}$ is the average value of the three bond angles of the first anion in Fig. 1. The spin polarization energy ΔE_p (eV) and the total magnetic moment m (μ_B) are also presented.

Systems	θ	$\overline{\theta}$	r_a (Å)	r_b (Å)	ΔE_p (eV)	m (μ_B)
V_{Be} in BeO	115.2	116.6	3.022	2.971	0.35	2.00
V_{Zn} in ZnO	116.0	116.7	3.647	3.588	0.04	1.71
V_{Zn} in ZnS	109.5	110.5	3.944	3.890	< 0.01	1.66
V_{Cd} in CdS	112.4	113.1	4.560	4.293	< 0.01	1.95
V_B in BN	114.1	114.1	2.798	2.822	0.19	3.00
V_{Al} in AlN	116.1	117.4	3.509	3.444	0.83	3.00
V_{Ga} in GaN	115.0	115.0	3.434	3.431	0.48	3.00
V_{Ga} in GaP	107.6	107.4	3.595	3.653	< 0.01	3.00

Table III. Calculated parameters of symmetry lowered atomic geometries. The atomic distances $r_{a'}$, $r_{b'}$, $r_{c'}$ and $r_{d'}$ are defined in Figure 5. ΔE_1 is the energy of the spin singlet (doublet) C_{3v} symmetry measured from the energy of the spin singlet (doublet) C_s symmetry in the case of II-VI (III-V) semiconductors.
$\Delta E_2 = \Delta E_p - \Delta E_1$ is the energy of the spin singlet (doublet) C_s symmetry measured from the energy of the spin triplet (quartet) C_{3v} symmetry in the case of II-VI (III-V) semiconductors.

Systems	type	$r_{a'}$ (Å)	$r_{b'}$ (Å)	$r_{c'}$ (Å)	$r_{d'}$ (Å)	ΔE_1 (eV)	ΔE_2 (eV)
V_{Zn} in ZnO	pairing	3.635	3.642	3.603	3.605	0.01	0.03
V_{Ga} in GaN	depairing	3.459	3.453	3.465	3.457	0.23	0.25
V_{Al} in AlN	depairing	3.550	3.549	3.482	3.481	< 0.01	0.83
V_{Be} in BeO	depairing	3.031	3.030	2.988	2.987	< 0.01	0.35

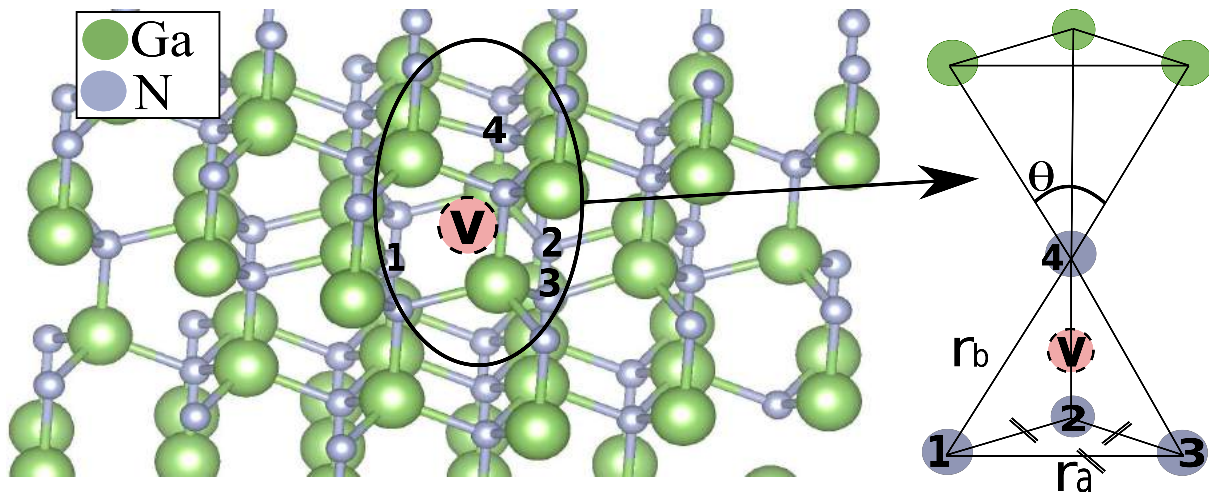

Fig. 1. Atomic structure of single cation vacancy of the C_{3v} symmetry (left-hand side). The atomic distances (r_a and r_b) and bond angles (θ) are defined (right-hand side) and these values are tabulated in Table I.

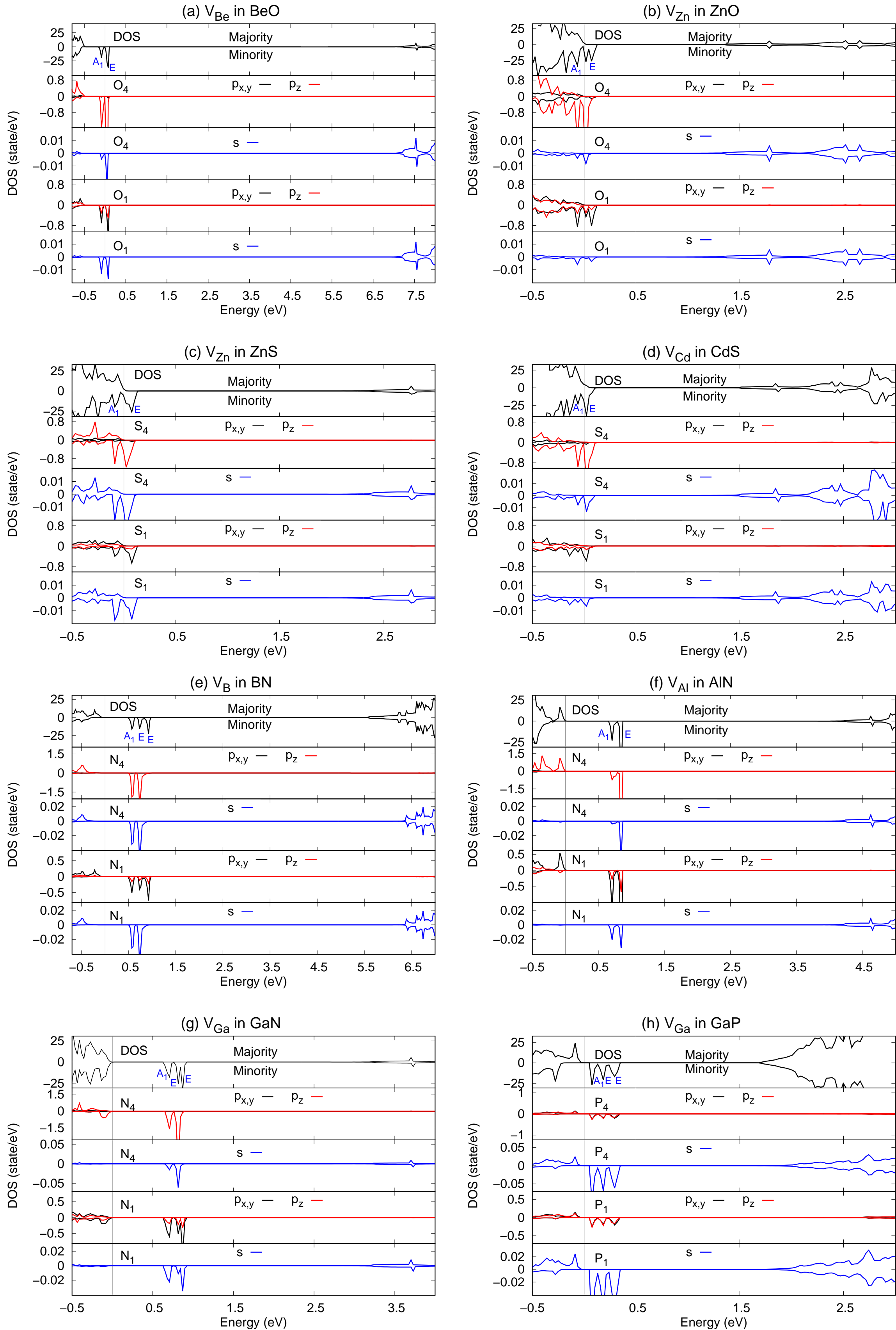

Fig. 2. DOS and PDOS of the 1st and 4th near anions which are defined in Figure 1. The vertical grey line represents the Fermi level. The results for (a)V_{Be} in BeO, (b)V_{Zn} in ZnO, (c)V_{Zn} in ZnS, (d)V_{Cd} in CdS, (e)V_B in BN, (f)V_{Al} in AlN, (g)V_{Ga} in GaN, and (h)V_{Ga} in GaP are shown.

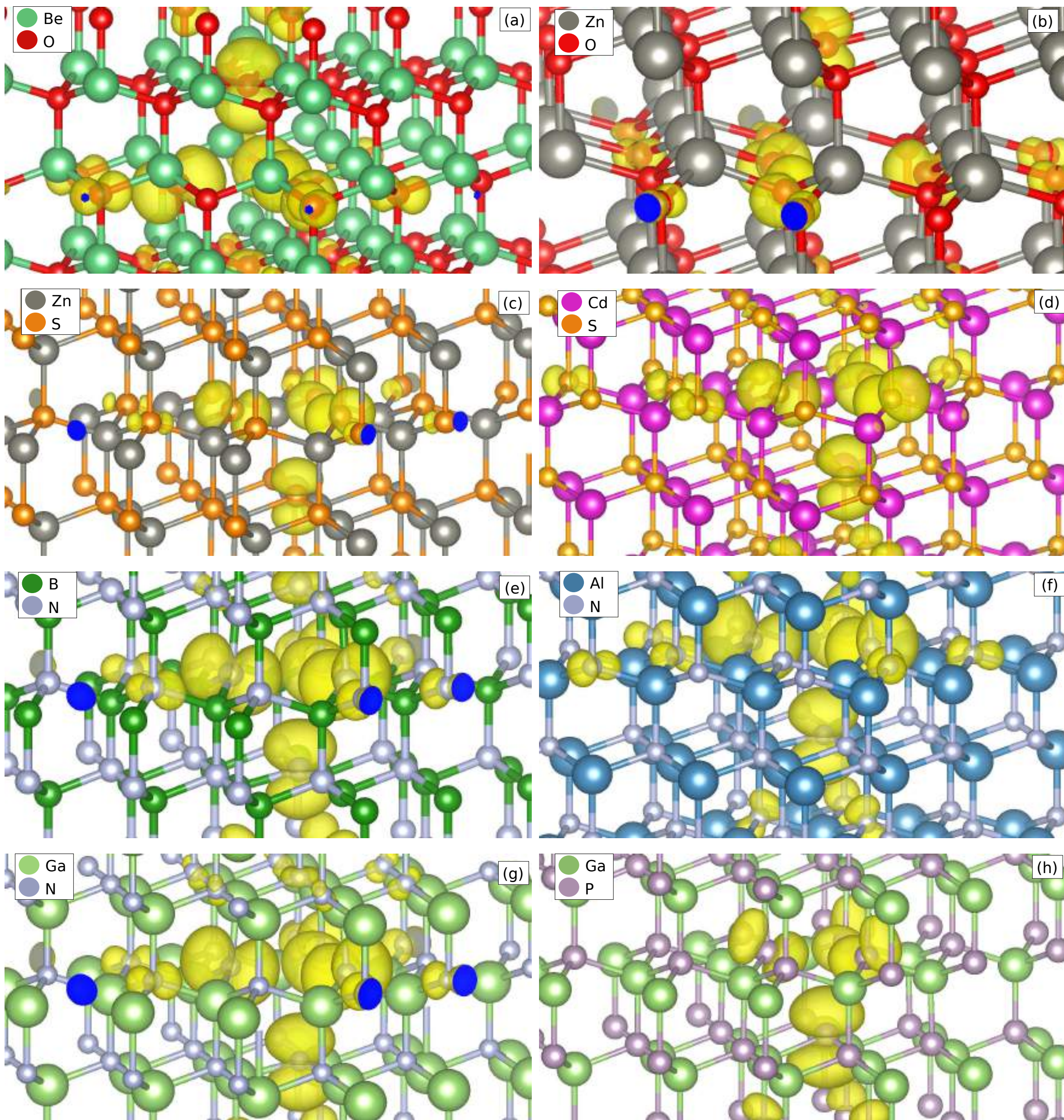

Fig. 3. Spin densities: (a)V_{Be} in BeO, (b)V_{Zn} in ZnO, (c)V_{Zn} in ZnS, (d)V_{Cd} in CdS, (e)V_{B} in BN, (f)V_{Al} in AlN, (g)V_{Ga} in GaN, and (h)V_{Ga} in GaP (The isovalues are set to be 0.001 electron /Å^3).

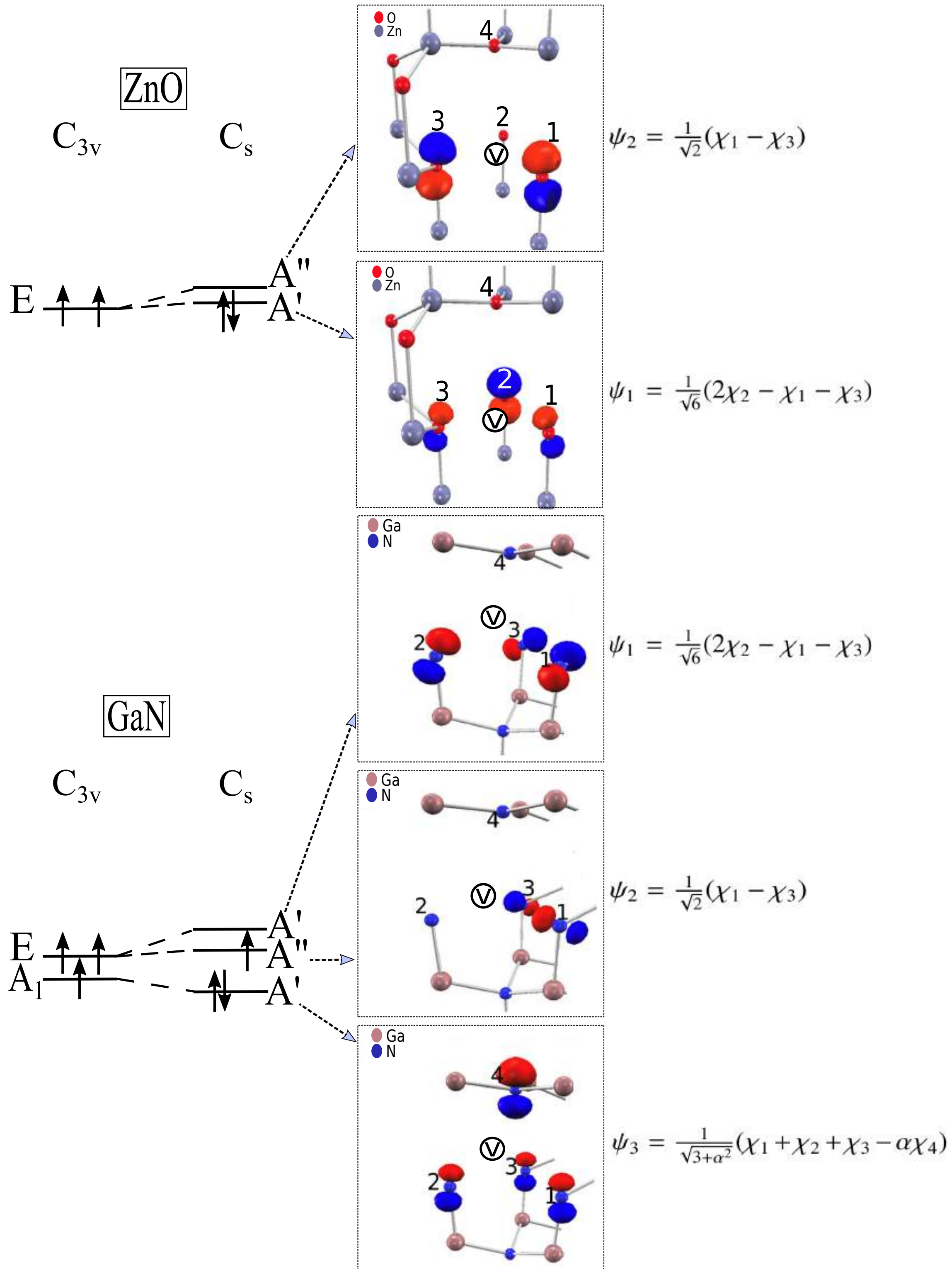

Fig. 4. Energy diagrams of the C_{3v} and C_s in the cases of ZnO and GaN. The red (blue) colors indicates positive (negative) amplitudes of the wavefunctions.

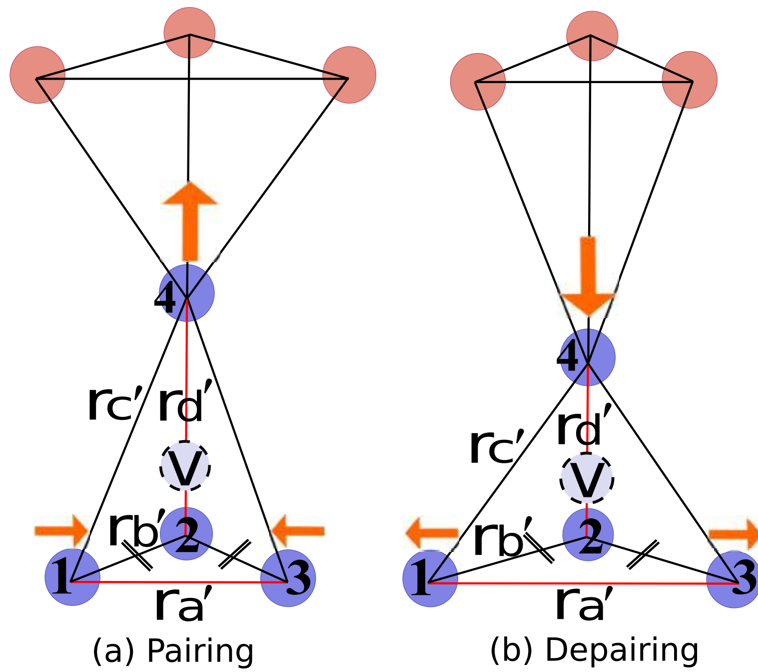

Fig. 5. Two types of symmetry lowering: (a) pairing and (b) depairing distortions.